Structure, Vol. 12, 361–370, March, 2004, ©2004 Elsevier Science Ltd. All rights reserved. DOI 10.1016/j.str.2004.02.010

Coenzyme Binding in F_{420}-Dependent Secondary Alcohol Dehydrogenase, a Member of the Bacterial Luciferase Family

Stephan W. Aufhammer,[1] Eberhard Warkentin,[2] Holger Berk,[1] Seigo Shima,[1] Rudolf K. Thauer,[1] and Ulrich Ermler[2,*]

[1]Max-Planck-Institut für terrestrische Mikrobiologie
Karl-von-Frisch-Straße
D-35043 Marburg

[2]Max-Planck-Institut für Biophysik
Marie-Curie-Straße 15
D-60439 Frankfurt am Main
Germany

Summary

F_{420}-dependent secondary alcohol dehydrogenase (Adf) from methanogenic archaea is a member of the growing bacterial luciferase family which are all TIM barrel enzymes, most of which with an unusual nonprolyl *cis* peptide bond. We report here on the crystal structure of Adf from *Methanoculleus thermophilicus* at 1.8 Å resolution in complex with a F_{420}-acetone adduct. The knowledge of the F_{420} binding mode in Adf provides the molecular basis for modeling F_{420} and FMN into the other enzymes of the family. A nonprolyl *cis* peptide bond was identified as an essential part of a bulge that serves as backstop at the *Re*-face of F_{420} to keep it in a bent conformation. The acetone moiety of the F_{420}-acetone adduct is positioned at the *Si*-face of F_{420} deeply buried inside the protein. Isopropanol can be reliably modeled and a hydrogen transfer mechanism postulated. His39 and Glu108 can be identified as key players for binding of the acetone or isopropanol oxygens and for catalysis.

Introduction

Methanogenesis is the final process of the anaerobic degradation of biomass performed by methanoarchaea (Thauer, 1998). One third of the methane is generally formed from CO_2 by reduction with H_2. In a few organisms, alcohols, either ethanol or isopropanol, can also serve as electron donors for CO_2 reduction. In methanogens, ethanol oxidation is catalyzed by a NADP-dependent alcohol dehydrogenase (Berk and Thauer, 1997), which belongs to the medium-chain alcohol dehydrogenases. Isopropanol oxidation is carried out by a coenzyme F_{420}-dependent secondary alcohol dehydrogenase (Adf) (Widdel and Wolfe, 1989), which does not belong to any of the known alcohol dehydrogenase families. F_{420} is a 5′-deazaflavin with a redox potential of −360 mV (Figure 1). Notably, in several eukaryotes, isopropanol oxidation to acetone is catalyzed by short-chain alcohol dehydrogenases using the $NADP^-$/NADPH system for hydride transfer (Jornvall et al., 1995).

Adf has been isolated from *Methanoculleus thermophilicus* and *Methanofollis liminatans* and has been kinetically characterized (Bleicher and Winter, 1991; Widdel and Wolfe, 1989). The enzyme catalyzes hydride transfer from or to the *Si*-face of F_{420} (Klein et al., 1996), as found for all characterized F_{420}-dependent enzymes (Thauer, 1998). The homodimeric enzyme is built up of subunits with a calculated molecular mass of 37.2 kDa. The Adf encoding genes from both organisms have been cloned, sequenced, and expressed in *Escherichia coli* (Berk, 1999). The heterologously produced enzyme was only partially soluble; most of it was isolated as inclusion bodies. The soluble fraction, however, contained Adf with high activity.

Amino acid comparisons revealed Adf to be related to F_{420}-dependent oxidoreductase from *Streptomyces* (33% sequence identity) (Peschke et al., 1995), F_{420}-dependent hydride transferase 1 from *Rhodococcus* (27%) (Heiss et al., 2002), F_{420}-dependent methylenetetrahydromethanopterin reductase (Mer) from methanogenic archaea (26%) (Nolling et al., 1995; Vaupel and Thauer, 1995), bacterial luciferase (LuxAB) (25%) (Baldwin et al., 1979), glucose-6-phosphate dehydrogenase from *Mycobacteria* (22%) (Purwantini and Daniels, 1998), and alkanesulfonate monoxygenase (SsuD) (22%) (van Der Ploeg et al., 1999) (Figure 2). From this enzyme family, referred to as the bacterial luciferase family, the F_{420}-dependent glucose-6-phosphate dehydrogenase from *Mycobacteria* has recently alerted more general interest (Choi et al., 2001; Stover et al., 2000), since the enzyme is involved in oxygen stress defense in the pathogenic bacteria.

LuxAB (Fisher et al., 1996), Mer (Shima et al., 2000), and SsuD (Eichhorn et al., 2002) of the bacterial luciferase family are structurally characterized and consist primarily of an $(\alpha\beta)_8$ barrel. While LuxAB and Mer contain an unusual nonprolyl *cis* peptide bond in strand β3, this characteristic feature is missing in SsuD. Unfortunately, none of the three enzymes were, until now, structurally determined in complex with its coenzyme, FMN (LuxAB and SsuD) or F_{420} (Mer). The coenzymes could, however, be approximately modeled into the structures either, as in the case of LuxAB, by computer assisted conformational search methods (Lin et al., 2001) or qualitatively on the basis of the flavin position found in other unrelated flavin-containing TIM barrel enzymes, such as FAD-containing MetF (Guenther et al., 1999) and FMN-containing enzymes: old yellow enzyme (Fox and Karplus, 1994), trimethylamine dehydrogenase (Lim et al., 1986), glycolate oxidase (Lindqvist, 1989), and dihydroorotate dehydrogenase A (Rowland et al., 1997). Another flavin-dependent TIM barrel enzyme with known crystal structure is the nonfluorescent protein (Moore and James, 1994). Despite its bacterial luciferase-like fold, the nonfluorescent protein deviates considerably from those of the bacterial luciferase family, in that the two FMN molecules have completely different binding sites.

The coenzyme F_{420} is only transiently associated with Adf in the catalytic reaction (K_m = 18 μM in the case of Adf from *M. liminatans*), like the other members of bacterial luciferase family. However, in the case where

*Correspondence: ulrich.ermler@mpibp-frankfurt.mpg.de

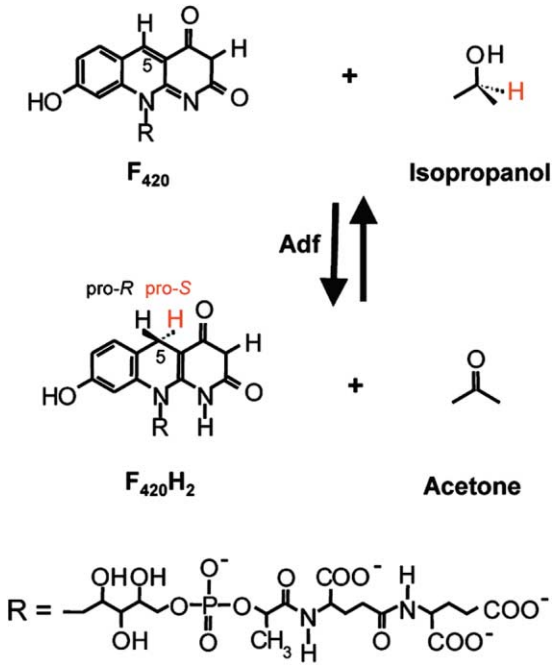

Figure 1. F_{420}-Dependent Alcohol Dehydrogenase Catalyzes the Oxidation of Isopropanol to Acetone with the Concomitant Reduction of F_{420} to $F_{420}H_2$

The enzyme is *Si*-face-specific with respect to the C5 atom of F_{420}. Coenzyme F_{420} is composed of a deazaflavin ring, a ribitol, a phosphate, a lactate, and two or more glutamates. The rest R in F_{420} is shown for F_{420}-2, the coenzyme present in *Methanoculleus*.

Adf was purified from the *M. thermophilicus* cells cultivated in the presence of 0.2% isopropanol in a 80% H_2/20% CO_2 atmosphere (see Experimental Procedures), the enzyme has been observed to copurify with F_{420}, indicating that F_{420} binds rather tightly to this enzyme. We therefore chose this enzyme preparation to characterize the cofactor binding mode in the bacterial luciferase family.

Results

Structure of Adf

The crystal structure of Adf has been resolved at 1.8 Å resolution in complex with a F_{420}-acetone adduct using the multiple isomorphous replacement method for phase determination (Table 1). The enzyme is present as a homodimer with a size of 75 Å × 50 Å × 50 Å (Figure 3A). Each monomer is basically built up of an $(\alpha\beta)_8$ barrel or TIM barrel fold according to triosephosphate isomerase (Banner et al., 1975), the first structurally elucidated protein of this architecture. The central strands of the $(\alpha\beta)_8$ barrel in Adf are arranged to form a funnel-shaped barrel broadened toward its C-terminal end, thereby creating a large roughly oval bottom (Figure 3). A similar TIM barrel core is found in LuxAB (Fisher et al., 1996), Mer (Shima et al., 2000), and SsuD (Eichhorn et al., 2002).

An unusual feature of the central β sheet is a bulge inserted into strand β3 exactly at the same position as described for LuxAB and Mer. This bulge that points into the interior of the TIM barrel is formed, in particular, by a nonprolyl *cis* peptide bond between Cys72 and Ile73. After the bulge, the direction of strand β3 changes by nearly 45° (Figure 4). The driving force for forming the energetically unfavorable nonprolyl *cis* peptide bond is difficult to grasp, although sequence and structural analysis clearly attribute a key function to the highly conserved Asp38. The carboxylate side chain of Asp38 is directed toward the bulge and would partly interfere with strand β3 if it would proceed straightforward. Moreover, the position of this carboxylate group is fixed by a salt bridge to Arg79 and by hydrogen bonds to the side chains of Tyr80 and Thr74, the latter stabilizing the conformation of the bulge (Figure 4).

The connecting segments between β strands and α helices of the TIM barrel core are mostly small, but four of them, named as insertion segments (IS) 1 to 4, are longer and are most likely of functional importance (Figure 3C). IS1 (Phe40–Gly52), following strand β2, consists of an extended loop without any secondary structure, and IS2 (Gly107–Pro120), following strand β4, is characterized by a small α helix. IS3 (Pro234–Asp286), following strand β6, is mainly composed of four short α helices and one β strand, which constitutes together with the prolonged strands β7 and β8 an additional three-stranded parallel β sheet nearly perpendicular to the central sheet. These three insertion regions are in tight contact to each other and cover the bottom of the C-terminal end of the TIM barrel (Figure 3C). IS4 (Gly141–Asp166), following helix α3 at the N-terminal side of the barrel, is attached parallel to helix α4.

The monomers of the dimer are related by a crystallographic 2-fold symmetry axis that is located parallel to the central strands (Figure 3A). Larger interface regions are formed between helix α2 and helix α2 of the symmetry-related partner, between helix α3 and helix α1, IS1, plus the loop following strand β3, and between IS4 and IS1 plus IS3. Altogether, the contact covers an area of 2215 Å^2, corresponding to about 16.4% of the surface area of the monomer (NACCESS; Hubbard et al., 1991). Notably, the same dimer arrangement was found in LuxAB, Mer, and SsuD. The dimer formation has, of course, a general stabilizing function, but structure analysis suggests additionally a direct function by fixing the conformations of IS1, IS2, and IS3, which are involved in F_{420} and substrate binding.

F_{420} Binding

F_{420} binds into a 15 Å long cavity that extends from the C-terminal end of the TIM barrel to the protein surface (Figure 3). The substituent of F_{420} consisting of a ribitol, a lactate, a phosphate, and two glutamates (Figure 1) is arranged perpendicular to the direction of the central strands in an elongated manner. The isoalloxazine ring is bound to Adf in a bent conformation with an angle of 26° between the peripheral rings (Figure 4). The coenzyme binding site is completely occupied by F_{420}, as indicated by roughly identical temperature factors (~21 Å^2) of the deazaflavin ring and its environment.

The deazaisoalloxazine head of F_{420} is positioned partly inside the barrel and is embedded into a pocket located at one side of the broadened bottom at the C-terminal

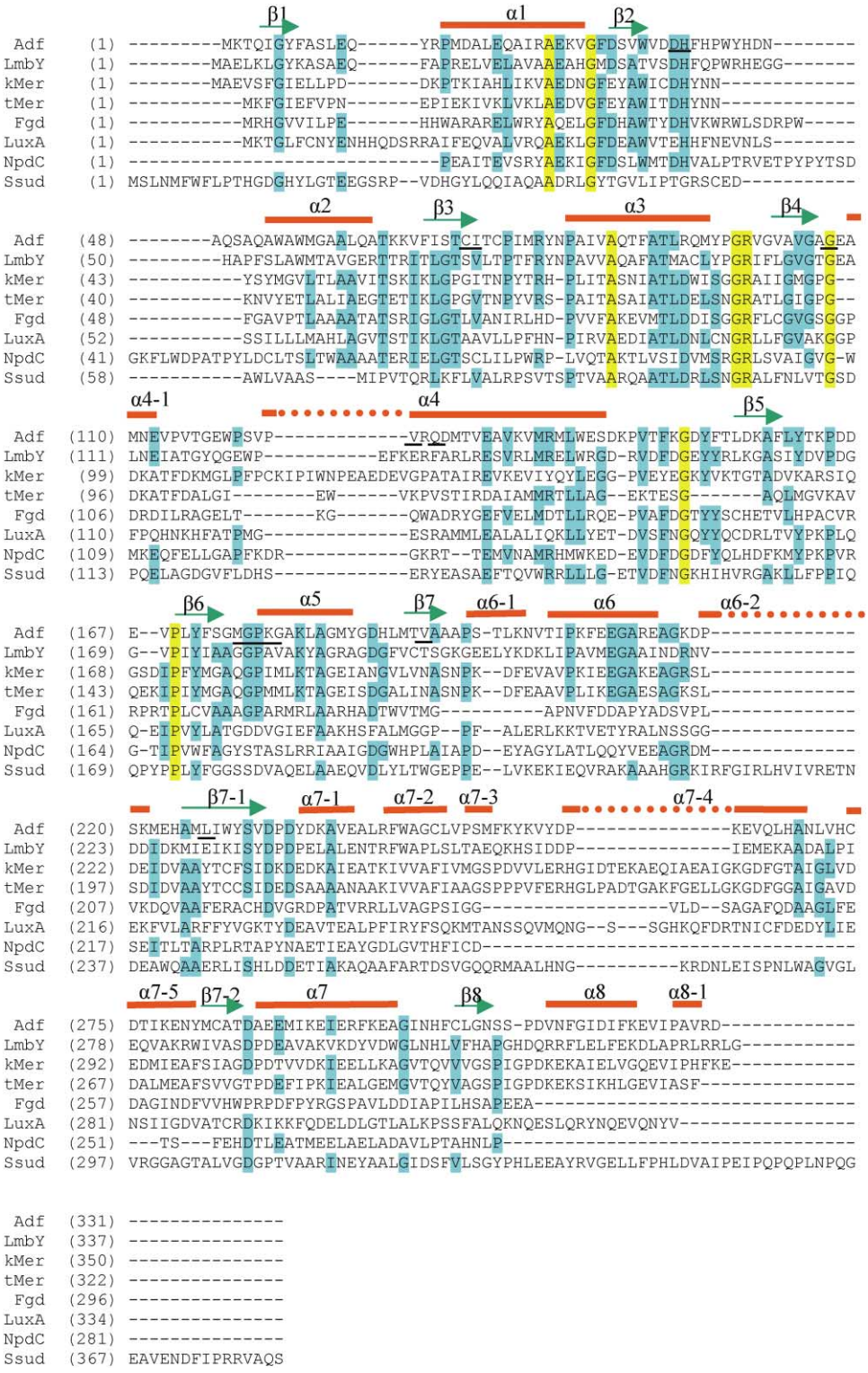

Figure 2. Sequence Alignment of the Bacterial Luciferase Family

A larger subfamily is characterized by a nonprolyl *cis* peptide bond; a smaller subfamily to which SsuD belongs does not contain such a bond. Identical residues are colored in yellow, and conserved residues are colored in blue. Arrows and bars above indicate the secondary structure assignment based on the Adf structure. Residues involved in F_{420} binding are underlined.

Table 1. Data Collection

Data Set	Native1	Native2	Pt1[a]	Pt2[a]	Hg1[a]	Pb1[a]
Resolution (Å)	2.6 (2.64–2.6)	1.8 (1.83–1.8)	3.0 (3.06–3.0)	3.0 (3.06–3.0)	3.0 (3.06–3.0)	3.0 (3.06–3.0)
Multiplicity	3.1(3.1)	3.9 (3.8)	2.3 (2.2)	2.3 (2.1)	2.6 (2.5)	3.2 (3.2)
Completeness (%)	96.2 (94.5)	99.2 (99.4)	94.2 (93.8)	82.0 (83.8)	94.0 (94.8)	90.9 (95.5)
I/σ_I	25.9 (5.9)	28.3 (3.2)	13.6 (5.3)	11.9 (3.5)	17.8 (7.0)	23.3 (10.3)
No. of crystals	3	7	1	1	1	1
R_{sym}, R_{merge} (%)[b]	7.9 (24.6)	6.7 (35.0)	12.1 (30.3)	12.4 (33.2)	9.8 (24.5)	9.6 (21.1)
R_{der} (%)[c] (5–10 Å)			10.6	12.4	7.5	4.5
Phasing power[d]			2.0	2.3	2.0	0.6

[a] Pt1: K_2PtCl_4, 0.9 mM (soaking concentration), 16 hours (soaking time); Pt2: di-μ-iodo-bis (ethylenediamine) di-platinum II nitrate (PIP), 0.3 mM, 24 hours; Hg1: MeHgOAc, 0.1 mM, 16 hours; Pb1: Me_3PbOAc, 0.9 mM, 16 hours.

[b] $R_{sym} = \Sigma_{hkl}\Sigma_i |I_i - \langle I\rangle|/\Sigma\langle I\rangle$; I_i, intensity of the i^{th} measurement per reflection hkl; $\langle I\rangle$, average intensity for a reflection hkl.

[c] $R_{der} = \Sigma_{hkl} ||F_P| - |F_{PH}||/\Sigma_{hkl}|F_p|$, $|F_P|$ and $|F_{PH}|$ are the structure factor amplitudes for the native protein and the heavy-atom derivatives.

[d] Phasing power is defined as $\langle |F_H|/\epsilon\rangle$; $\epsilon = |F_{PH} - |F_P + F_H||$ is the residual lack of closure. F_H is the calculated heavy-atom structure factor amplitude, and F_{PH} and F_P are the structure factors with and without heavy atoms.

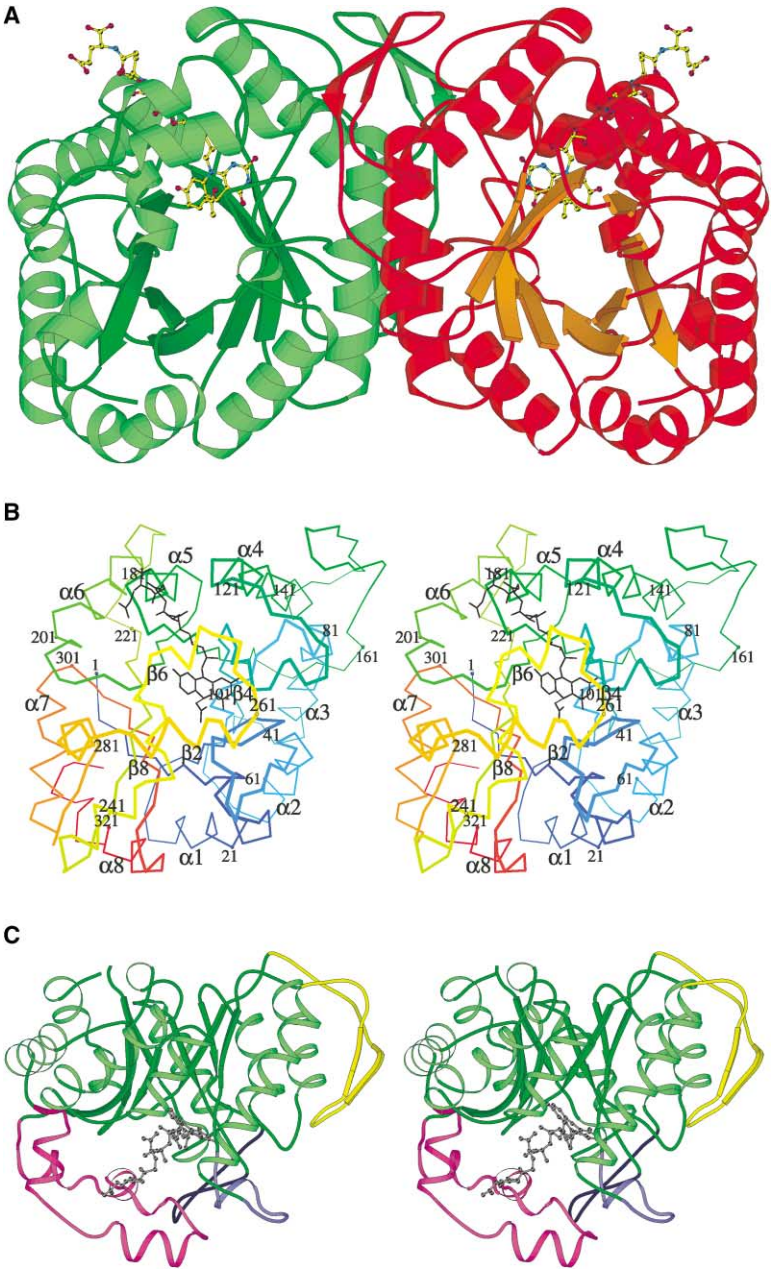

Figure 3. Structure of Adf from *Methanoculleus thermophilicus*

(A) Ribbon diagram of the dimer that shows the TIM barrel architecture of the monomer. The interface between the monomers is formed by three peripherical α helices and the insertion segments.

(B) Stereo representation of the C_α chain of the Adf monomer.

(C) Stereo plot of the Adf monomer (rotated 90° compared to [B]). The representation focuses on the conformation of the insertion regions (IS 1 to 4 in blue, sky-blue, magenta, and yellow) that are crucial for substrate binding and for the formation of the active site.

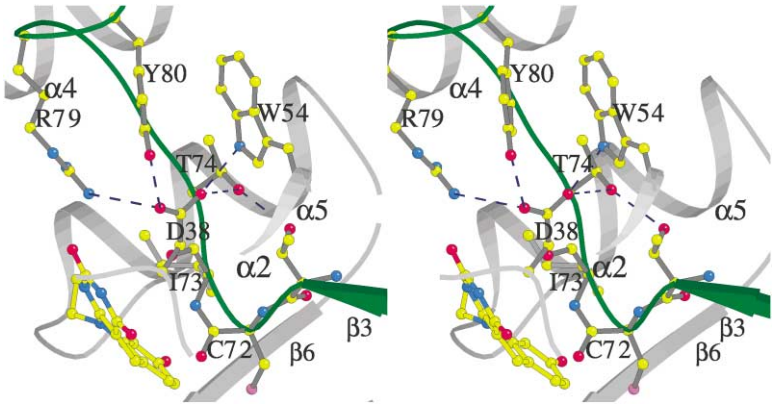

Figure 4. The Nonprolyl *cis* Peptide Bond in Adf

The nonprolyl *cis* peptide bond between Cys72 and Ile73 is an essential constituent of a bulge that is directed toward the F_{420} binding site, causing a bent conformation of the deazaisoalloxazine ring. The well-conserved Asp38, which would partly interfere with a straight course of strand β3, is strongly linked to the polypeptide chain and stabilizes the bulge. These favorable interactions might compensate for the energy lost when forming the nonprolyl *cis* peptide bond.

end. The three-membered ring system is flanked by strands β2 and β6, and its *Re*-face is attached to strands β3 and β5 (Figure 3). The so-called butterfly conformation is maintained at the *Si*-face by fixing the pyrimidine and hydroxybenzyl wings via His39 and Glu108 and by Val193 and Ile227, respectively. The central pyridine ring is kept in its position outside the plane by the nonprolyl *cis* peptide oxygen of Cys72 and by the side chain of Ile73 pointing toward its *Re* side and acting as a backstop (Figure 4). Incorporation of a *cis* proline at position 73 would substantially press the deazaflavin ring out of its binding site, indicating the functional necessity of a nonprolyl *cis* peptide bond. Interestingly, nonprolyl *cis* peptide bonds are rarely found in proteins and always have a specific function (Jabs et al., 1999). The isoalloxazine ring is anchored to the protein matrix by several interactions taking the amphipatic nature of the isoalloxazine ring into account (Figure 5A). Except for His39 and Ser173, hydrogen bonds are only formed to main chain atoms, providing a rigid coenzyme binding mode. A comparison between the Adf-derived and the calculated binding site (Lin et al., 2001) resulted in a very similar binding position. However, the orientation of the isoalloxazine ring substantially deviates, such that the bulge serves as a backstop in the Adf-based model and as a hydrogen bond mediator in the calculated model.

The substituent of F_{420} is buried inside the protein until the first glutamate and contributes significantly to coenzyme binding involving, in particular, IS1, IS2, and IS3 (Figure 5A). The second glutamate is solvent exposed and highly flexible. Notably, residue 176, which interacts with the phosphate group, has to be a glycine to avoid a clash with F_{420}. This residue is not conserved in the FMN-dependent luciferase and perhaps provides a general distinctive feature for F_{420} and FMN-dependent members of this family (Figure 2).

Acetone Binding

Additional electron density was rather unexpectedly found at the *Si*-face of F_{420} and was determined to be isopropanol or acetone (Figures 3 and 5B). Several models with and without acetone or isopropanol, either covalently bound or in an unbound state, were refined. The resulting electron density maps at 1.8 Å resolution clearly support the presence of an F_{420}-acetone adduct. The distance between the C1 atom of acetone and the C5 atom of F_{420} was refined to 1.5 Å, and the arrangement of the C1, C2, C3, and O atoms is clearly planar. The substrate binding pocket completely buried inside the enzyme is formed by the deazaflavin ring and side chains of strands β1, β2, β6, and β7 and of IS1, IS2, and IS3. These side chains comprising Phe8, His39, Trp43, Glu108, Val193, Trp229, Trp246, Cys249, and Phe255 are mainly bulky and hydrophobic, but a few are also polar and apparently play an important functional role (see below).

The binding of acetone is characterized by the interactions between its carbonyl oxygen and the polypeptide side chains (Figure 5B). The oxygen atom is in an ideal distance for hydrogen bond formation to the carboxylate group of Glu108, protruding from strand β4, to the imidazole ring of His39, and to the indol group of Trp43, the latter residues originating from the loop following β3. The carboxylate group of Glu108 and the imidazole group of His39 are kept in place via hydrogen bonds to the amide group of Asn111 and to the carbonyl group of His41, respectively. Trp43 is embedded in a hydrophobic pocket formed by Met210, Gly248, Cys249, Val251, Met254, Phe255, and Val265. Interestingly, the side chains of His39 and Glu108 are 3 Å apart, but a hydrogen bond can only be formed upon breaking the bond to the oxygen of acetone and rotating the imidazole ring (Figure 5B). Notably, the imidazole ring of His39 is also in van der Waals contact to the carboxylate group of Glu12, which is hydrogen bonded to Asp37. This latter residue, Asp37, is solvent accessible and thus capable of proton transfer to the outside of this protein (Figure 5B). It is conceivable that Glu12 is protonated, since it is in a rather hydrophobic environment.

Discussion

Flavin-Dependent TIM Barrel Structures

Adf is characterized by a TIM barrel fold, an unusual nonprolyl *cis* peptide bond, and its specificity for the deazaflavin F_{420}, which acts as a coenzyme instead of a prosthetic group. These properties are characteristic for most members of the bacterial luciferase family (Figure 2). Within this family, only SsuD (and some very related enzymes) does not contain the constituting nonprolyl *cis* peptide bond. The other structurally known flavin-dependent TIM barrel enzymes bind flavin as a

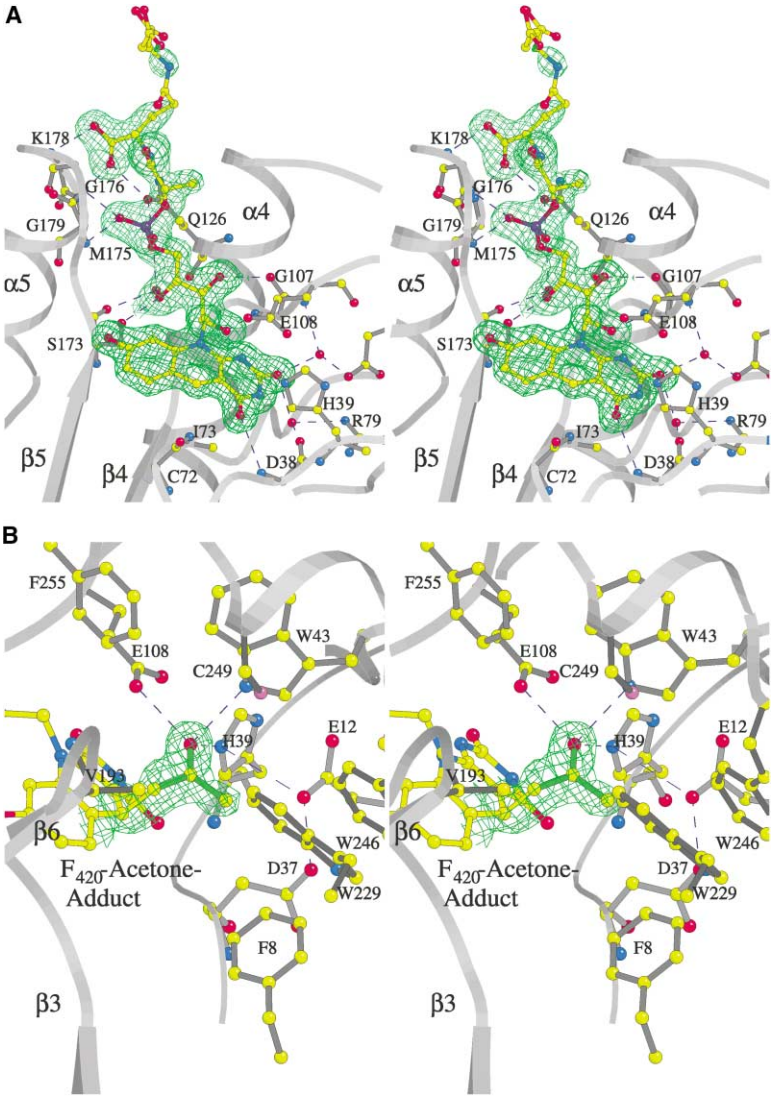

Figure 5. Stereo Plot Showing the Interactions between the Coenzyme Molecule—F_{420}—and the Enzyme and the Relative Positions of the F_{420} and Acetone Moieties of the F_{420}-Acetone Adduct

(A) F_{420} is bound into a 15 Å long cavity extending from the C-terminal end of the TIM barrel to the protein surface. It is linked to the protein matrix by 11 direct hydrogen bonds, mainly to main chain atoms. The negatively charged phosphate group is hydrogen bonded to the amide nitrogen of Gln126 and to the peptide nitrogens of Met175 and Gly176. The first glutamate of F_{420} is fixed by helix α5, as the partially positive charge of its N-terminal end interacts with the negative charge of the carboxylate group.

(B) The acetone as part of the F_{420}-acetone adduct binds into a predominantly hydrophobic pocket at the *Si*-face of F_{420}. Residues His39, Glu108, and Trp43 are crucial for binding of the carbonyl oxygen of acetone. The hydroxyl oxygen of isopropanol probably binds to the same position and serves as an anchor for modeling the substrate.

prosthetic group and have no sequence similarity to the bacterial luciferase family.

According to a primary structure alignment, the residues contacting F_{420} are not conserved (Figure 2) in the luciferase family, reflecting the low overall sequence identity, the use of main chain atoms to provide polar interactions, and the possibility of equivalently exchanging hydrophobic contact residues. The sole exception in the nonprolyl *cis* peptide family is the strictly conserved His39 whose imidazole side chain is involved in F_{420} binding and substrate binding as well as catalysis (see below). Surprisingly, conserved residues were found in linker segments between the helices and strands at the N-terminal side of the barrel, suggesting that they might be involved in fine-tuning the directions of the strands. For example, a hydrogen bond is formed between the strictly conserved residues Thr64 and Arg99 to adjust strands β3 and β4, which are both involved in F_{420} binding (Figure 2).

In contrast to residues involved in flavin binding, the amino acids surrounding the nonprolyl *cis* peptide bond are better conserved. This allows a clear discrimination between the SsuD subfamily and the nonprolyl *cis* peptide subfamily, and the definition of a general fingerprint (together with His39) for the larger group of the luciferase family. A major role is assigned to the highly conserved Asp38 (in luciferase a glutamate) that stabilizes the bulge on one hand and would partly interfere with a straight course of strand β3 on the other. Asp38 is strongly fixed in its position, in particular, by a salt bridge to a positively charged residue at position 79, either arginine or histidine (Figures 2 and 3). The optimal binding situation for Asp38 is speculated to be the driving force for forming the energetically unfavorable nonprolyl *cis* peptide bond that results in the formation of a bulge. The residues of the bulge are less well conserved, although they reveal several common features. Residue 71 is either a proline or a threonine, residue 72 is rather variable, residue 73 is either a isoleucine or a valine, and residue 74 is mostly a threonine or a branched aliphatic amino acid (Figure 2). Altogether, the following consensus sequence can be derived: D/E-H-x(20-30)-I/L-S/G-x-I/V/A-x5-R/H.

Formation of the F_{420}-Acetone Adduct

Adf was structurally characterized in complex with an F_{420}-acetone adduct. The surprising formation of a cova-

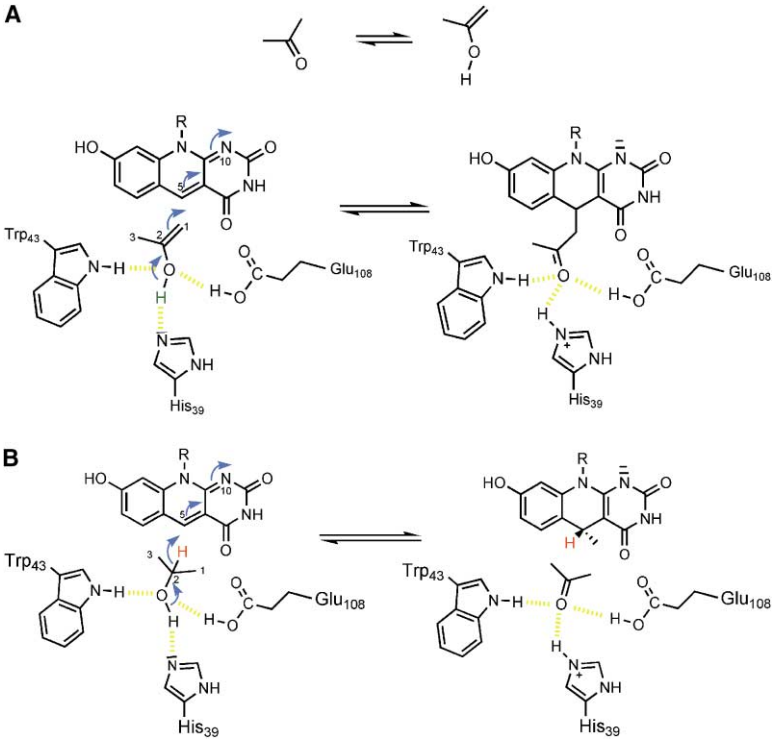

Figure 6. Proposed Mechanism of F_{420}-Acetone Formation and of Isopropanol Oxidation

(A) The reaction between acetone and oxidized F_{420} can be understood on the basis of the nucleophilic attack of the C1 atom of acetone onto the C5 atom of F_{420}. The C1 atom is electron rich, as seen in the enol or enolate tautomere of acetone.

(B) Hydride transfer from the C2 atom of acetone to the C5 atom of the *Si* side of the F_{420}. His39 is postulated to be the general catalytic base that abstracts a proton from isopropanol, whereas the protonated Glu108 and Trp43 stabilize the partly generated alcoholate anion in the transition state.

lent bond between the atoms C5 of F_{420} and C1 of acetone can be mechanistically explained considering the nucleophilic character of the C1 atom, especially in the enolate form of acetone. The enol form is only present in minor amounts ($K_{eq} = 1.5 \times 10^{-7}$) in water (Figure 6A), but in the protein the keto/enol tautomerization equilibrium might be substantially shifted (Benach et al., 1999). Due to the adjacent residues His39 and Glu108 that can serve as hydrogen donors and acceptors, structural analysis favors binding of a hydroxyl group as compared to an oxo atom. His39 would be optimally placed to serve as general acid to protonate the keto group of acetone, and simultaneously, Glu108 might accept a proton from the C1 atom placed 3.7 Å away from the carboxyl group (Figure 5B).

Accordingly, the electron-rich C1 atom nucleophilically attacks the electrophilic C5 atom of the oxidized F_{420} and generates the adduct. His39 can additionally function as a general base by accepting a proton from the hydroxyl group during the carbon-carbon linkage (Figure 6A). An analogous covalent NADP-acetone adduct was previously found for *Drosophila* short-chain alcohol dehydrogenase (Benach et al., 1999). The postulated mechanism for its biosynthesis exactly corresponds to that described for the formation of the F_{420}-acetone adduct. The formation of such an adduct tighly blocks the active site cavity of Adf and results in a dead-end enzyme.

As indicated above and outlined in Figure 6A, both acetone and oxidized F_{420} are required for the formation of the F_{420}-acetone adduct in the active site of Adf. This explains why adduct-containing Adf was primarily found in cells incubated under N_2/CO_2 after growth on H_2/CO_2 and isopropanol. Acetone accumulates during growth. Then, during incubation under N_2/CO_2, coenzyme F_{420} is oxidized via an F_{420}-dependent hydrogenase. This interpretation is substantiated by the finding that the specific activity of Adf decreased continuously during a 2 day incubation of cells under N_2/CO_2. Finally, the specific activity was estimated to be lower than 10% of Adf purified from cells before induction of adduct formation.

Substrate Binding and Hydride Transfer

The position of the acetone as part of the F_{420}-acetone adduct does not exactly correspond to that of isopropanol prior to the reaction. Nevertheless, reliable modeling of isopropanol into its binding site is straightforward, provided that the observed position of the acetone oxygen is also the binding site for the isopropanol oxygen forming the same interactions with the polypeptide matrix (Figure 5B). Moreover, isopropanol must be bound in a manner to orient the hydrogen of its C2 atom toward the C5 atom of the isoalloxazine (Figure 6B) like the C1 atom of acetone in the F_{420}-acetone adduct (Figure 6A). According to these restraints, the C3 atom of isopropanol is in a similar position as the C3 atom of the observed F_{420}-acetone adduct and in van der Waals contact to Phe8, Glu12, Asp37, His39, Trp229, Trp246, and the deazaflavin ring. The C1 atom is in van der Waals contact to Phe43, Trp229, and Cys249. In this orientation, the C3 atom is completely surrounded by protein atoms, while there is space for at least one additional methyl group in front of the C1 atom. This structural finding is in agreement with kinetic data that Adf can oxidize isopropanol, isobutanol, and isopentanol but cannot oxidize larger secondary alcohols (Bleicher and Winter, 1991). The specificity for these secondary alcohols comes from the bulky and hydrophobic side chains. Thus, site-directed amino acid exchanges can be used

to design binding sites with different specificities for new substrates.

The position of F_{420} and isopropanol defines the active site for hydride transfer in the interior of Adf that is completely shielded from bulk solvent. As observed in many enzymes, the polypeptide framework keeps the reaction partners in a favorable relative position. Accordingly, the distance of 2.9 Å between the C2 atom of isopropanol and the C5 atom of F_{420} is optimal for hydride transfer. Two structural features in Adf appear to be functionally crucial and warrant additional discussion. First, the reduced deazaflavin ring is present in a bent conformation (Figure 4) which is, according to molecular orbital calculations, energetically favorable for the reduced but not for the oxidized state (Hall et al., 1987). If the butterfly conformation of F_{420} is approximately maintained in the oxidized state, the three-membered ring is strained and the concomitant higher energy decreases the activation energy for reaching the transition state. Formation and stabilization of the butterfly conformation is attributed to the bulge that is constituted by a nonprolyl *cis* peptide bond in which the carbonyl oxygen serves as backstop (Figure 4). Second, the polypeptide environment around the isopropanol hydroxyl group allows abstraction of a proton and the subsequent stabilization of the partially negatively charged oxygen in the transition state (Figure 6B). From structural studies, the function of His39 or Glu108 as general bases cannot be definitely identified. Adjacent histidine and glutamate residues are normally considered to be charged at neutral pH, but His39 and especially Glu108 are buried in a hydrophobic region such that an uncharged state of one or both residues seems energetically attainable. We postulate a mechanism based on the uncharged state, but further structural and functional studies with enzymes containing site-specific amino acid exchanges are essential for clarifying the mechanism (see Figure 6B). Accordingly, if His39 acts as a general catalytic base for accepting the hydroxyl hydrogen of isopropanol, the partially formed alcoholate anion would then be neutralized by hydrogen bonds to Trp 43 and protonated Glu108. Moreover, the distance between the carboxylate oxygen of Glu108 and the N10 atom of the deazaflavin is 3.4 Å, so the protonation of the N10 atom by Glu108 is possible. Interestingly, the oxidation of a hydroxyl group can be enzymatically catalyzed rather differently. In zinc-dependent alcohol dehydrogenases, the transition energy is predominantly decreased by coordinating the alcohol anion to a Zn^{2+} (Eklund et al., 1982), and in secondary alcohol dehydrogenases (Benach et al., 1999) and in L-3-hydroxyacyl-CoA dehydrogenase (Barycki et al., 1999) by abstracting a proton using the strong bases tyrosylate and histidine, the latter being enhanced by a nearby glutamate.

Experimental Procedures

Preparation of the Enzyme

Methanoculleus thermophilicus (strain TCI; DSMZ 3915) deposited in the Deutsche Sammlung von Mikroorganismen (Braunschweig, Germany) was grown at 55°C in the presence of 0.2% isopropanol in an 80% H_2/20% CO_2 atmosphere for 5 days up to an optical density of 0.2. Then the culture was supplemented with 0.5% isopropanol in an 80% N_2/20% CO_2 atmosphere, further incubated without growing at 55°C for 2 days, and then harvested (Berk, 1999; Widdel and Wolfe, 1989). F_{420}-dependent alcohol dehydrogenase (Adf) was isolated under anaerobic conditions using ammonium sulfate precipitation and a Phenyl-Sepharose HiLoad 26/10 column as described (Klein et al., 1996). For purification, buffers were supplemented with 15 mM mercaptoethanol. About 2.5 mg pure enzyme, with a specific activity of 7.7 U/mg at 40°C under standard assay conditions (Widdel and Wolfe, 1989), could be isolated from 1 liter of culture. When the cells were harvested after 5 days of growth, before 2 days incubation under N_2/CO_2, the purified Adf had a specific activity of 50 U/mg. However, the highly active enzyme preparations did not crystallize under the conditions employed. The same was true for heterologously produced Adf in *E. coli*, which also had a specific activity of 50 U/mg.

The purified enzyme with the specific activity of 7.7 U/mg was unstable in low ionic strength buffers. Stabilization could be achieved by supplementing solutions of Adf with 40 mM sodium phosphate (pH 7), 200 mM sodium sulfate, 10 mM 2-propanol, and 15 mM mercaptoethanol (Bleicher and Winter, 1991). Under these conditions, the enzyme could be stored for several days without considerable loss of activity.

Crystallization and Data Collection

Shortly before crystallization, the stabilized enzyme was transferred into a buffer containing 10 mM MOPS/KOH (pH 7) and 15 mM mercaptoethanol. The protein concentration was 15 mg/ml. The search for initial crystallization conditions was carried out with Hampton Research crystallization kits (Jancarik and Kim, 1991) at a temperature of 4°C using the hanging drop vapor diffusion method. Crystals could be obtained with NaCl as precipitant. They grew best in a drop consisting of 2 μl of enzyme solution (12 mg/ml) and 2 μl of reservoir solution consisting of 0.1 M citrate-NaOH (pH 4), 1% PEG 8000, and 3.6 M NaCl. The obtained space group of $C222_1$ and the unit cell parameters of a = 86.8 Å, b = 156.3 Å, and c = 60.2 Å are compatible with one monomer per asymmetric unit (Matthews, 1968). The solvent content is 51.6%. Since all applied cryoprotectants damaged the crystals substantially, data collection was performed at temperatures of 4°–8°C using crystals mounted in fine glass capillaries. The high radiation sensitivity of the crystals required data collection from several crystals to obtain a complete data set to higher resolution. For efficient data collection, STRATEGY (Ravelli et al., 1997) was applied. Data sets Native1, Pt1, Pt2, Hg1, and Pb1 were measured at a temperature of 8°C using a Rigaku rotating Cu anode and a MarResearch image plate detector. Native data to 1.7 Å resolution (Native2) were collected at Max-Planck beam line BW6 at the Deutsches Elektronen Synchroton in Hamburg. Processing and scaling of the reflections were performed with the HKL suite (Otwinowski and Minor, 1997). The statistics of the data sets are summarized in Table 1.

Phase Determination and Model Building

Phases of Adf crystals were determined by the method of multiple isomorphous replacement on the basis of four heavy atom derivatives (Table 1). Crystallographic calculations were achieved within the CCP4 program suite (CCP4, 1994). The difference Patterson map of the derivatives Pt1 and Hg1 could be interpreted using SHELXD (Schneider and Sheldrick, 2002). Heavy-atom coordinate refinement, phase determination, and the search for further heavy-atom binding sites by difference Fourier techniques were preformed in SHARP (De La Fortelle and Bricogne, 1997). Phase statistics are listed in Table 1, the overall figure of merit being 0.54 in the resolution range 100–2.6 Å. After solvent flattening (SOLOMON; Abrahams and Leslie, 1996) calculated in the space group $C222_1$, the quality of the electron density was sufficiently high to incorporate a polypeptide model with O (Jones et al., 1991) using the density skeletonization option (MAPMAN; Kleywegt and Jones, 1996). Model building was facilitated by automatically fitting the segments ranging from Ser70 to Gly150 and from Pro252 to Thr285 using MAID (Levitt, 2001).

Model Refinement and Quality of the Model

Refinement was performed using CNS (Brunger et al., 1998), applying standard protocols and manual correction using O (Jones et al., 1991). Water atoms were selected automatically in two rounds;

a few were picked manually. Two peaks were assigned to Cl^- on the basis of their coordination and interatomic distances, and one was assigned to K^+. The R values converged to R = 0.155 and R_{free} = 0.187 in the resolution range 20–1.8 Å (0.205 and 0.236, respectively, between 1.86 and 1.80 Å) with the model including 330 amino acids, 1 F_{420}-acetone adduct, and solvent molecules (146 H_2O, 2 Cl^-, 1K^+). The average displacement factor is B = 26.5 $Å^2$, and the root-mean-square deviation from the standard values (Engh and Huber, 1991) of the bond lengths is 0.016 Å and of the angles is 1.7°. The quality of the model was checked within CNS and PROCHECK (Laskowski et al., 1993). The Ramachandran plot showed all of the nonglycine or nonproline residues except one in the most favored (91.7%) or additionally allowed regions (8.0%).

Figure Preparation

Figures 3, 4, and 6 were generated using MOLSCRIPT (Kraulis, 1991), and Figure 5 was generated using BOBSCRIPT (Esnouf, 1997).

Acknowledgments

This work was supported by the Max-Planck-Gesellschaft and the Graduiertenkolleg "Protein Function at the Atomic Level" of the DFG. We thank Hartmut Michel for continuous support, Erica Lyon for reading the manuscript, and the staff of Max-Planck beamline BW6 at DESY, Hamburg, in particular Gleb Bourenkov, for help during data collection.

Received: October 2, 2003
Revised: November 14, 2003
Accepted: November 29, 2003
Published: March 9, 2004

References

Abrahams, J.P., and Leslie, A.G.W. (1996). Methods used in the structure determination of bovine mitochondrial F-1 ATPase. Acta Crystallogr. D *52*, 30–42.

Baldwin, T.O., Ziegler, M.M., and Powers, D.A. (1979). Covalent structure of subunits of bacterial luciferase: NH_2-terminal sequence demonstrates subunit homology. Proc. Natl. Acad. Sci. USA *76*, 4887–4889.

Banner, D.W., Bloomer, A.C., Petsko, G.A., Phillips, D.C., Pogson, C.I., Wilson, I.A., Corran, P.H., Furth, A.J., Milman, J.D., Offord, R.E., et al. (1975). Structure of chicken muscle triose phosphate isomerase determined crystallographically at 2.5 angstrom resolution using amino acid sequence data. Nature *255*, 609–614.

Barycki, J.J., O'Brien, L.K., Bratt, J.M., Zhang, R., Sanishvili, R., Strauss, A.W., and Banaszak, L.J. (1999). Biochemical characterization and crystal structure determination of human heart short chain L-3-hydroxyacyl-CoA dehydrogenase provide insights into catalytic mechanism. Biochemistry *38*, 5786–5798.

Benach, J., Atrian, S., Gonzalez-Duarte, R., and Ladenstein, R. (1999). The catalytic reaction and inhibition mechanism of *Drosophila* alcohol dehydrogenase: observation of an enzyme-bound NAD-ketone adduct at 1.4 A resolution by X-ray crystallography. J. Mol. Biol. *289*, 335–355.

Berk, H. (1999). F_{420} und NADP-abhängige Alkohol-Dehydrogenasen und $F_{420}H_2$:NADP-Oxidoreduktasen aus methanogenen Archaea: Struktur und Stereospezifität. Ph.D. thesis, Philipps-Universität Marburg/Lahn, Marburg/Lahn, Germany.

Berk, H., and Thauer, R.K. (1997). Function of coenzyme F_{420}-dependent NADP reductase in methanogenic archaea containing an NADP-dependent alcohol dehydrogenase. Arch. Microbiol. *168*, 396–402.

Bleicher, K., and Winter, J. (1991). Purification and properties of F_{420}- and NADP(+)-dependent alcohol dehydrogenases of *Methanogenium liminatans* and *Methanobacterium palustre*, specific for secondary alcohols. Eur. J. Biochem. *200*, 43–51.

Brunger, A.T., Adams, P.D., Clore, G.M., DeLano, W.L., Gros, P., Grosse-Kunstleve, R.W., Jiang, J.S., Kuszewski, J., Nilges, M., Pannu, N.S., et al. (1998). Crystallography & NMR system: a new software suite for macromolecular structure determination. Acta Crystallogr. D Biol. Crystallogr. *54*, 905–921.

CCP4 (Collaborative Computational Project 4) (1994). The CCP4 suite: programs for protein crystallography. Acta Crystallogr. D *50*, 760–763.

Choi, K.P., Bair, T.B., Bae, Y.M., and Daniels, L. (2001). Use of transposon Tn5367 mutagenesis and a nitroimidazopyran-based selection system to demonstrate a requirement for fbiA and fbiB in coenzyme F(420) biosynthesis by *Mycobacterium bovis* BCG. J. Bacteriol. *183*, 7058–7066.

De La Fortelle, E., and Bricogne, G. (1997). Maximum likelihood heavy-atom parameter refinement for multiple isomorphous replacement and multiwavelength anomalous diffraction methods. Methods Enzymol. *276*, 472–494.

Eichhorn, E., Davey, C.A., Sargent, D.F., Leisinger, T., and Richmond, T.J. (2002). Crystal structure of *Escherichia coli* alkanesulfonate monooxygenase SsuD. J. Mol. Biol. *324*, 457–468.

Eklund, H., Samama, J.P., and Wallen, L. (1982). Pyrazole binding in crystalline binary and ternary complexes with liver alcohol dehydrogenase. Biochemistry *21*, 4858–4866.

Engh, R.A., and Huber, R. (1991). Accurate bond and angle parameters for X-ray protein structure refinement. Acta Crystallogr. *A47*, 392–400.

Esnouf, R.M. (1997). An extensively modified version of MOLSCRIPT that includes greatly enhanced coloring capabilities. J. Mol. Graph. *15*, 133–138.

Fisher, A.J., Thompson, T.B., Thoden, J.B., Baldwin, T.O., and Rayment, I. (1996). The 1.5-Å resolution crystal structure of bacterial luciferase in low salt conditions. J. Biol. Chem. *271*, 21956–21968.

Fox, K.M., and Karplus, P.A. (1994). Old yellow enzyme at 2 Å resolution: overall structure, ligand binding, and comparison with related flavoproteins. Structure *2*, 1089–1105.

Guenther, B.D., Sheppard, C.A., Tran, P., Rozen, R., Matthews, R.G., and Ludwig, M.L. (1999). The structure and properties of methylenetetrahydrofolate reductase from *Escherichia coli* suggest how folate ameliorates human hyperhomocysteinemia. Nat. Struct. Biol. *6*, 359–365.

Hall, L.H., Bowers, M.L., and Durfor, C.N. (1987). Further consideration of flavin coenzyme biochemistry afforded by geometry-optimized molecular orbital calculations. Biochemistry *26*, 7401–7409.

Heiss, G., Hofmann, K.W., Trachtmann, N., Walters, D.M., Rouviere, P., and Knackmuss, H.J. (2002). npd gene functions of *Rhodococcus* (*opacus*) *erythropolis* HL PM-1 in the initial steps of 2,4,6-trinitrophenol degradation. Microbiol. *148*, 799–806.

Hubbard, S.J., Campbell, S.F., and Thornton, J.M. (1991). Molecular recognition. Conformational analysis of limited proteolytic sites and serine proteinase protein inhibitors. J. Mol. Biol. *220*, 507–530.

Jabs, A., Weiss, M.S., and Hilgenfeld, R. (1999). Non-proline cis peptide bonds in proteins. J. Mol. Biol. *286*, 291–304.

Jancarik, J., and Kim, S.-H. (1991). Sparse matrix sampling: a screening method for crystallization of proteins. J. Appl. Crystallogr. *24*, 409–411.

Jones, T.A., Zou, J.Y., Cowan, S.W., and Kjeldgaard, M. (1991). Improved methods for building protein models in electron density maps and the location of errors in these models. Acta Crystallogr. *A47*, 110–119.

Jornvall, H., Persson, B., Krook, M., Atrian, S., Gonzalez-Duarte, R., Jeffery, J., and Ghosh, D. (1995). Short-chain dehydrogenases/reductases (SDR). Biochemistry *34*, 6003–6013.

Klein, A.R., Berk, H., Purwantini, E., Daniels, L., and Thauer, R.K. (1996). Si-face stereospecificity at C5 of coenzyme F_{420} for F_{420}-dependent glucose-6-phosphate dehydrogenase from *Mycobacterium smegmatis* and F_{420}-dependent alcohol dehydrogenase from *Methanoculleus thermophilicus*. Eur. J. Biochem. *239*, 93–97.

Kleywegt, G.J., and Jones, T.A. (1996). xdlMAPMAN and xdlDATAMAN—programs for reformatting, analysis and manipulation of biomacromolecular electron-density maps and reflection data sets. Acta Crystallogr. D Biol. Crystallogr. *52*, 826–828.

Kraulis, P.J. (1991). MOLSCRIPT: a program to produce both detailed and schematic plots of protein structures. J. Appl. Crystallogr. *24*, 946–950.

Laskowski, R.A., MacArthur, M.W., Moss, D.S., and Thornton, J.M. (1993). PROCHECK: a program to check the stereochemical quality of protein structures. J. Appl. Crystallogr. *26*, 283–291.

Levitt, D.G. (2001). A new software routine that automates the fitting of protein X-ray crystallographic electron-density maps. Acta Crystallogr. D Biol. Crystallogr. *57*, 1013–1019.

Lim, L.W., Shamala, N., Mathews, F.S., Steenkamp, D.J., Hamlin, R., and Xuong, N.H. (1986). Three-dimensional structure of the iron-sulfur flavoprotein trimethylamine dehydrogenase at 2.4-Å resolution. J. Biol. Chem. *261*, 15140–15146.

Lin, L.Y., Sulea, T., Szittner, R., Vassilyev, V., Purisima, E.O., and Meighen, E.A. (2001). Modeling of the bacterial luciferase-flavin mononucleotide complex combining flexible docking with structure-activity data. Protein Sci. *10*, 1563–1571.

Lindqvist, Y. (1989). Refined structure of spinach glycolate oxidase at 2 Å resolution. J. Mol. Biol. *209*, 151–166.

Matthews, B.W. (1968). Solvent content of protein crystals. J. Mol. Biol. *33*, 491–497.

Moore, S.A., and James, M.N. (1994). Common structural features of the luxF protein and the subunits of bacterial luciferase: evidence for a (beta alpha)8 fold in luciferase. Protein Sci. *3*, 1914–1926.

Nolling, J., Ishii, M., Koch, J., Pihl, T.D., Reeve, J.N., Thauer, R.K., and Hedderich, R. (1995). Characterization of a 45-kDa flavoprotein and evidence for a rubredoxin, two proteins that could participate in electron transport from H_2 to CO_2 in methanogenesis in *Methanobacterium thermoautotrophicum*. Eur. J. Biochem. *231*, 628–638.

Otwinowski, Z., and Minor, W. (1997). Processing of X-ray diffraction data collected in oscillation mode. Methods Enzymol. *276*, 307–326.

Peschke, U., Schmidt, H., Zhang, H.Z., and Piepersberg, W. (1995). Molecular characterization of the lincomycin-production gene cluster of *Streptomyces lincolnensis* 78–11. Mol. Microbiol. *16*, 1137–1156.

Purwantini, E., and Daniels, L. (1998). Molecular analysis of the gene encoding F_{420}-dependent glucose-6-phosphate dehydrogenase from *Mycobacterium smegmatis*. J. Bacteriol. *180*, 2212–2219.

Ravelli, R.B.G., Sweet, R.M., Skinner, J.M., Duisenberg, A.J.M., and Kroon, J. (1997). STRATEGY: a program to optimize the starting angle and scan range for X-ray data collection. J. Appl. Crystallogr. *30*, 551–554.

Rowland, P., Nielsen, F.S., Jensen, K.F., and Larsen, S. (1997). The crystal structure of flavin containing enzyme dihydroorotate dehydrogenase from *Lactococcus lactis*. Structure *5*, 239–252.

Schneider, T.R., and Sheldrick, G.M. (2002). Substructure solution with SHELXD. Acta Crystallogr. D Biol. Crystallogr. *58*, 1772–1779.

Shima, S., Warkentin, E., Grabarse, W., Sordel, M., Wicke, M., Thauer, R.K., and Ermler, U. (2000). Structure of coenzyme F(420) dependent methylenetetrahydromethanopterin reductase from two methanogenic archaea. J. Mol. Biol. *300*, 935–950.

Stover, C.K., Warrener, P., VanDevanter, D.R., Sherman, D.R., Arain, T.M., Langhorne, M.H., Anderson, S.W., Towell, J.A., Yuan, Y., McMurray, D.N., et al. (2000). A small-molecule nitroimidazopyran drug candidate for the treatment of tuberculosis. Nature *405*, 962–966.

Thauer, R.K. (1998). Biochemistry of methanogenesis: a tribute to Marjory Stephenson. Microbiol. *144*, 2377–2406.

van Der Ploeg, J.R., Iwanicka-Nowicka, R., Bykowski, T., Hryniewicz, M.M., and Leisinger, T. (1999). The *Escherichia coli* ssuEADCB gene cluster is required for the utilization of sulfur from aliphatic sulfonates and is regulated by the transcriptional activator Cbl. J. Biol. Chem. *274*, 29358–29365.

Vaupel, M., and Thauer, R.K. (1995). Coenzyme F_{420}-dependent N5,N10-methylenetetrahydromethanopterin reductase (Mer) from *Methanobacterium thermoautotrophicum* strain Marburg. Cloning, sequencing, transcriptional analysis, and functional expression in *Escherichia coli* of the mer gene. Eur. J. Biochem. *231*, 773–778.

Widdel, F., and Wolfe, R.S. (1989). Expression of secondary alcohol dehydrogenase in methanogenic bacteria and purification of the F_{420}-specific enzyme from *Methanogenium thermophilum* strain TCI. Arch. Microbiol. *152*, 322–328.

Accession Numbers

The atomic coordinates for coenzyme F_{420}-dependent alcohol dehydrogenase Adf from *M. thermophilicus* have been deposited in the Protein Data Bank with the accession code 1RHC.